JOM, Vol. 73, No. 12, 2021
https://doi.org/10.1007/s11837-021-04925-2

Processing, Characterization, and Properties of α-Al_2O_3-AA2900 Composites for Aerospace Brake Pad Applications

P. ASHWATH,[1] M. ANTHONY XAVIER ,[1,3] and ANDRE DL BATAKO[2]

1.—Vellore Institute of Technology, Vellore 632014, India. 2.—Liverpool John Moores University, Liverpool, UK. 3.—e-mail: manthonyxavior@vit.ac.in

Replacing high-strength frictional materials with lightweight composite alternatives is currently a global challenge for researchers. In this work, aluminum alloy (AA2900)-based metal-matrix composites reinforced with 6 wt.% α-alumina were fabricated then subjected to T6 heat treatment followed by case hardening. The resulting composite samples exhibited improved hardness, strength behavior, and stress–strain behavior along with good ductility and formability when microwave sintered. Good microstructural bonding was observed for all samples, which can be attributed to the finer α-Al_2O_3 particulates used as the reinforcement and the microwave sintering process. The mechanical and wear properties of the composites were compared with existing aerospace brake pad material. Data for wear characteristics versus the number of landings for the existing brake pad material were considered as the benchmark data, and the feasibility of replacing it with the developed composites was evaluated.

INTRODUCTION

Particle-reinforced aluminum alloy-based metal-matrix composites have attracted attention from researchers as engineering materials due to their outstanding comprehensive mechanical properties such as strength-to-weight ratio and superior hardness compared with the parent aluminum alloy. However, the microstructural and bulk properties of such composites depend on various experimental parameters, such as the pressure used for compaction, the dwell time during compaction, the duration of sintering, and heating rate, as investigated by Abbass et al.[1] Based on similar work, Alexander et al.[2] reported that surface modification of alumina-reinforced aluminum composites could result in surface characteristics required in the aerospace field. The optimization and validation of the strength and tribological properties of developed aluminum alloy metal-matrix composites (AAMMCs) depend on the strength–microstructural relation as reported by Bobic et al.[3] and Dilipet al.[4]. Elanchezhian et al.[5] reported that several matrix materials can be used together to achieve desired bulk microstructural properties that differ from those of monolithic alloy materials. Funatani et al.[6] mentioned that comprehensive inspection and validation of such surface modification of composites at the matrix–reinforcement level are necessary to understand their bulk behavior. In this regard, Gao et al.[7] stated that processed composites exhibited this behavior and that addition of reinforcement (i.e. ceramic particles) to a lighter metal matrix contributes to enhancing the bulk microstructure. Ikumapayi et al.[8] reported the rapid progress in the discipline of fiber materials for lightweight applications, the structure of the matrix–reinforcement interface, bonding, and the distinctive final bulk microstructural properties of the developed composite. Kavi et al.[9] quantified the dependence of the microstructure bulk properties of developed composite on various experimental factors, such as the pressure used for compaction, the dwell time during compaction, the duration of sintering, and the heating rate. Kurt et al.[10] mentioned that nearly all load-bearing aluminum alloys currently in use

(Received June 14, 2021; accepted September 16, 2021; published online October 15, 2021)

have copper as a major alloying element, which provides the essential strength and tribological properties required after surface processing to match the requirements of aerospace and space exploration applications. Madeva et al.[11] and Manish et al.[12] argued that addition of harder ceramic materials in particle form can enhance the surface characteristics of the developed composites and eventually lead to lightweight materials that could be considered as good replacements for use in aerospace applications. Miran et al.[13] and Murtaza et al.[14] reported that surface modification and bulk treatment of aluminum composites using nonconventional methods could lead to improvements in their surface or subsurface properties such as hardness and tribological characteristics. Prasad et al.[15] and Prem et al.[16] reported friction applications of lightweight composites in brake pads, interface piston rings and piston pins, tiny gear components for aerospace use, brake discs, and cast engineering parts with promising and acceptable performance for use in the automotive and aerospace industries. Huang et al.[17] and Subhash et al.[21] found that comprehensive inspection and validation of the integrity of composites at the matrix–reinforcement level are necessary to understand their bulk behavior. Toozandehjani et al.[23] stated that various parameters affect the formation of such materials, including the characteristics of the reinforcement particulates added, i.e., average size, shape, and weight percentage, as well as the metal matrix, i.e., average grain size, types of alloying elements, and precipitates formed during the fabrication process. The reviews by Logesh et al.[27] and Granesan et al.[28] described the mechanical validation and characterization data, revealing the significant control exerted by the morphology of the reinforcements on the properties of the final composite. The work presented herein focuses on the fabrication and processing of AAMMC to achieve enhanced strength–tribological combinations depending on the processing conditions applied. Most existing aircraft brake pad materials are made of ferrous (Fe)-based and copper (Cu)-based matrix materials which are quite dense and heavier in nature. Identifying lightweight alternate materials to replace heavier brake pad materials and characterizing their performance under braking conditions are thus necessary. AAMMC with added Al_2O_3 exhibited a good strength–tribological combination as a potential frictional material to replace existing brake friction materials used during braking of aircraft under dry conditions because of its enhanced resistance to wear at higher temperature and excellent thermal conductivity (i.e., heat dissipation).

EXPERIMENTAL PROCEDURES

The current study focuses on the development and validation of aluminum alloy composites fabricated by a powder metallurgy route and synthesized by microwave processing. The matrix material used for fabricating the composites was aluminum alloy 2900 (AA2900) purchased from AMPAL Inc. USA, while the reinforcement material was 6 wt.% α-Al_2O_3 [26] procured from Carborundum Universal Limited, Kerala, India. A digital balance with calibrated accuracy of 0.001 g was used to measure the quantity of powder to be used for fabrication of the samples, to avoid weight mismatch between the powders. To remove moisture from the weighed powder mixture, it was loaded into a hot-air oven with capability of 400°C for 60 min. High-energy planetary ball milling for 30 min at 200 rpm in acetone medium was used to blend the powder mixture and achieve homogeneous mixing of matrix and reinforcement with a ball-to-powder ratio of 10:1. The resulting mixture was dried in an electrical oven at 100°C [24]. A hydraulic press with capacity of 500 tons was used for uniaxial pressing of the samples by compacting at 450 MPa. Different die sets for compacting the desired specimens, including tensile samples, compressive samples, wear samples, and samples for microstructural characterization, were fabricated with a compaction holding duration of 12 min. The compaction die set was made of AISI D2 steel containing tungsten carbide as inner core walls. A compaction rate of around 2 tons per min was chosen. Zinc stearate was used as solid lubricant to coat the inner walls of the die and thus prevent the powder mixture from cold welding to the die walls. The compacted green compacts were sintered in a microwave sintering furnace under controlled nitrogen atmosphere at 495°C with a heating rate of 50°C. The maximum operation capacity of the microwave furnace was around 1000°C at the maximum power of 10 kW with a magnetron frequency of 2.45 GHz and dwell temperature accuracy of 1°C. The sintered composites were further solution-treated and quenched in a cold water bath and further artificially aged in an electrical oven with a maximum capacity of 400°C. Solution treatment and aging are included in the standard T6 heat treatment procedure applied for aluminum alloys (Fig. 1). After microwave processing, the synthesized T6 composites were further subjected to post bulk processing such as case hardening by pack carburizing (Fig. 2). Pack carburizing of T6-treated composites was performed in a sealed crucible filled with pulverized charcoal and barium carbonate mixture. Solution treatment for carburizing on T6 composite was performed at 500°C for a duration of 6 h. Supplementary Table S1 presents the process parameters applied for microwave case hardening. For solution treatment, a microwave method was used. High-resolution scanning electron microscopy was applied to

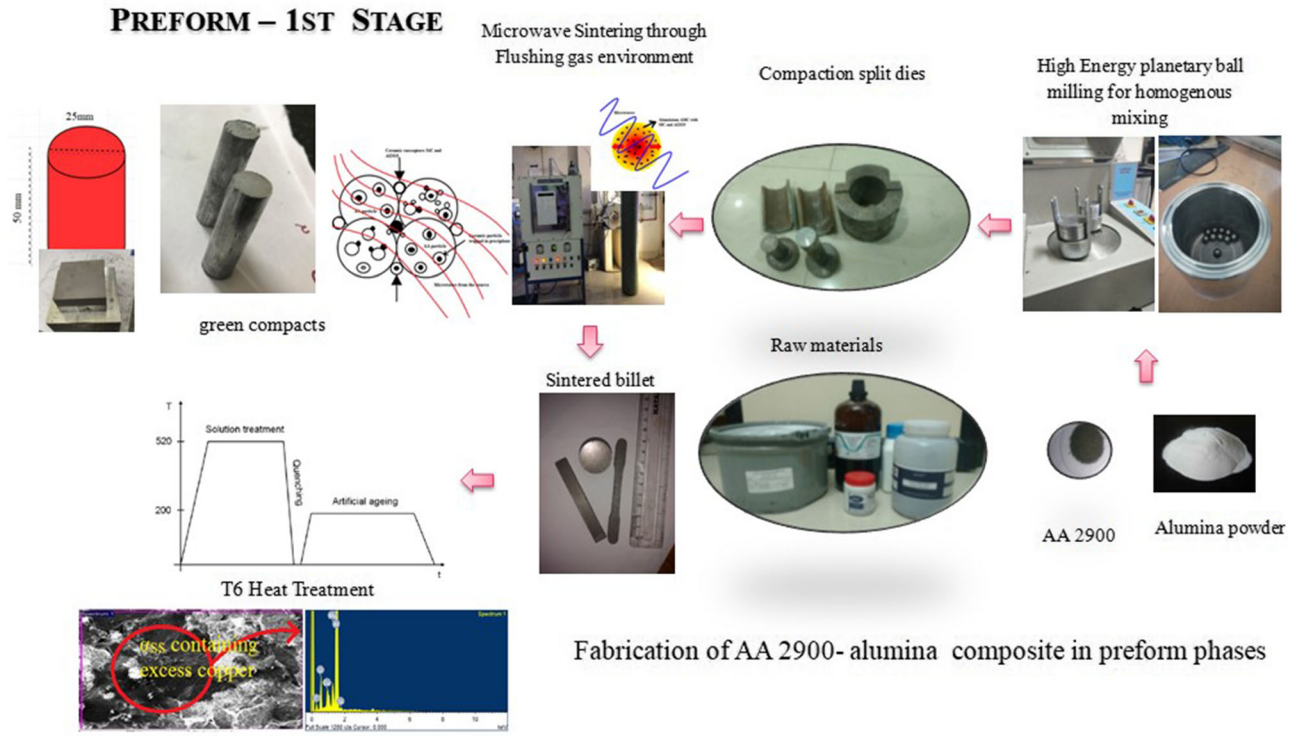

Fig. 1. Schematic of powder metallurgy route followed by T6 heat treatment.

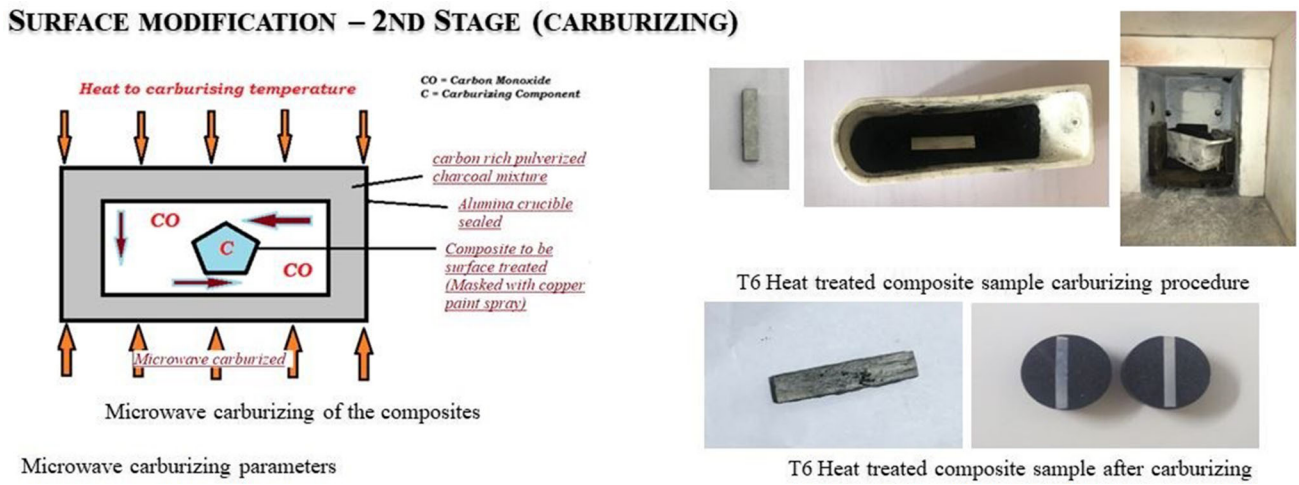

Fig. 2. Schematic of microwave case-hardening setup and mechanism.

study the microstructural integrity of the processed AAMMC samples. To enable clear microstructural study, the mirror-polished samples were etched using Keller's agent.

ASTM standard B962-17 was used for density measurements according to the Archimedes principle. Rockwell hardness was measured using standard ASTM E18 to determine the surface hardness of the samples by indenting with a 1/16 mm steel ball under 100 kgf. Standard ASTM E9 was chosen for compressive tests of the obtained samples (25 mm diameter, 50 mm height) in an Instron testing machine at a strain rate of 0.75 mm/min. ASTM standard B925-03 was used to perform shear testing on samples at a rate of 0.1 mm/min. All test results are the average for five samples per test, to ensure consistency. The high-temperature wear performance of the samples was tested using a pin-on-disc setup with maximum pin heating of 500°C using AAMMC pins with dimensions of 5 mm in cross-section and 50 mm in height. All wear and friction tests were repeated five times to provide confidence in the results. High-temperature wear testing was performed using a total distance of 5000 m, calculated from the runway of landing aircraft

with a total testing time of around 12 min in each trail. Wear testing was carried out in the realistic operating temperature range from 300°C to 450°C.

A handheld x-ray florescence analyzer was used to confirm the alloying elements and their percentage in the AA 2900 matrix (Supplementary Table S2). α-Al_2O_3 content of 3 wt.%, 6 wt.%, and 9 wt.% was used to reinforce the matrix, and the particle size for both powder materials was around 10 μm. Figure 3(a) presents a high-resolution scanning electron microscopy (HRSEM) image of the as-received powder, confirming its near-spherical shape. Figure 3(b) presents HRSEM micrographs of the as-received α-Al_2O_3. The x-ray powder diffraction (XRD) data in Fig. 3(c) confirm that the as-received alumina particles exhibited reflection peaks corresponding to the d spacings of hkl lattice planes 012, 116, 104, 113, and 110.

RESULTS AND DISCUSSION

Process Validation

To meet the challenging performance requirements of brake pads used in aerospace applications, secondary operations including bulk treatment or surface modification were applied to the AAMMC materials to improve their wear and friction properties, as well as case hardening to improve the surface characteristics to match the wear performance of existing brake pad materials. To achieve successful case hardening, the diffusion mechanism of carbon to the aluminum matrix in the fabricated T6-AA 2900 6 wt.% α-Al_2O_3 must be studied. Sahoo et al.[17] studied a similar carbon diffusion mechanism based on the graphene impregnation method to improve the surface properties of the developed composite. Manish et al.[12] reviewed the importance of adding carbon to the softer aluminum matrix and its composites to achieve the requirements of high-strength applications. In this regard, it has also been suggested that carbon diffusion to depths up to 500 μm can be achieved but is challenging, beyond which further improvements of the surface properties was not observed. Snihirova et al.[19] reported that carbon coating on the surface of aluminum composites resulted in the diffusion of a certain amount of carbon into the substrate, thereby improving the surface hardness and surface wear characteristics of the coating as observed after failure during the testing process. The aluminum–

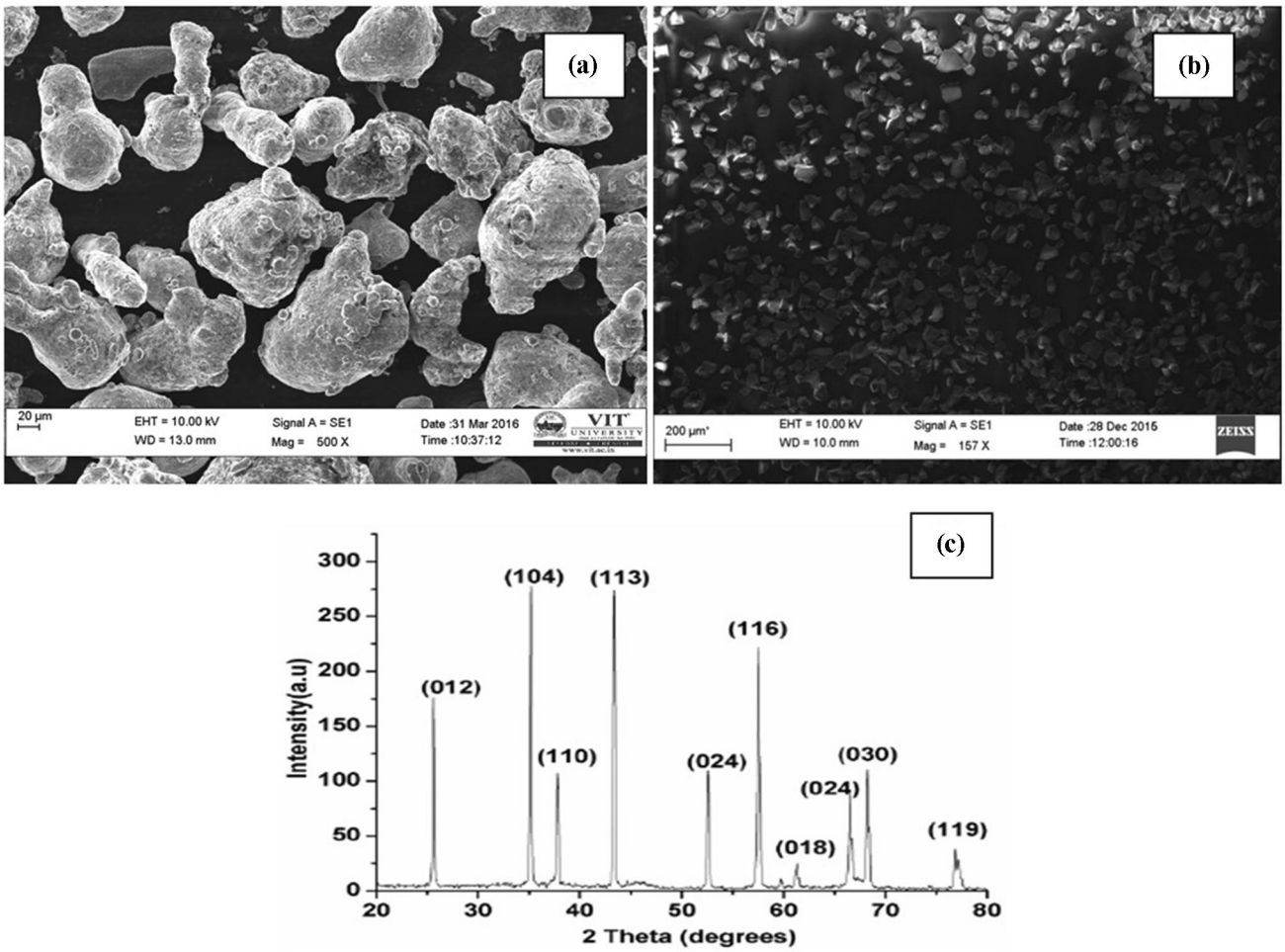

Fig. 3. HRSEM micrographs of (a) AA 2900 powder particle and (b) α-Al_2O_3, and (c) XRD of α-Al_2O_3.

carbon phase diagram is presented in Fig. 4. Along with the solubility, the depth of diffusion is also monitored for the AAMMC materials after both processes to evaluate their influence on the final properties.

Inspection of Fig. 4 reveals that the solubility also depends on the diffusion coefficient, thus purely being determined by the duration and temperature of the process. In the diffusion process, atoms diffuse through the solid matrix to form precipitates that can strengthen the composite, as reported in an aluminum matrix subjected to other processes by Prasad et al.[15]. The diffusion process thus results in precipitate strengthening of the matrix material to improve its properties. The amount and rate of diffusion of atoms can be measured empirically using Eq. (1).

$$\mathrm{J} = \mathrm{Flux} = \frac{\mathrm{Molesdiffusing}}{(\mathrm{surfacearea})\,(\mathrm{time})} = \frac{\mathrm{Mol}}{\mathrm{Cm^2S}} = \frac{\mathrm{Kg}}{\mathrm{M^2S}} \tag{1}$$

For case hardening of the solution-treated aluminum, a temperature of around 500°C was used for a duration of 6 h. Pack carburizing was performed by a microwave technique. The diffusion process is time/temperature dependent. The relation between the time and temperature of the diffusion process is expressed by Eq. (2), which was also applied in the research carried out by Sharma et al.[18]. Tracie[24] reported that a greater amount of carbon diffusion was observed in composites that are heated on the surface, which is driven by the activation energy of the surface towards enhancement of the diffusion coefficient. The reported temperature of around 600°C was achieved by applying a friction stir welding process on the composite, resulting in enhanced surface properties similar to and in agreement with the current findings. Murtaza et al.[14] reported that carburization of aluminum could be achieved by the plasma focus method where high-energy carbon ions from low energy (i.e., 1.45 kJ) are focused on the surface to initiate their diffusion on the surface.

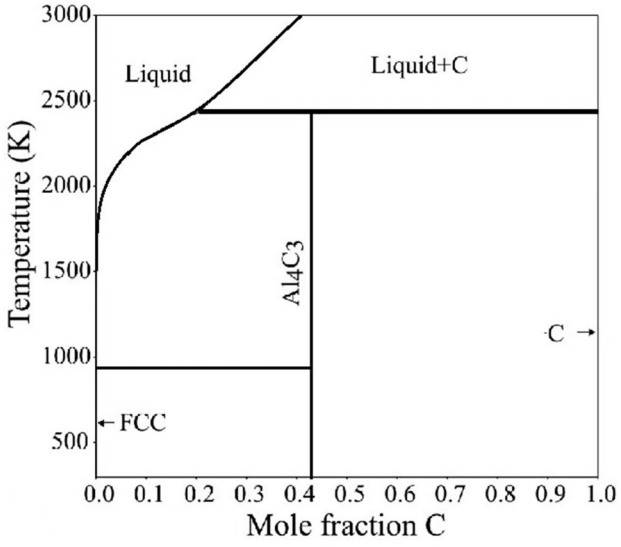

Fig. 4. Solubility graphs for aluminum alloy system: aluminum–carbon [15].

$$D = D_0 \exp -\frac{Q_d}{RT} \tag{2}$$

where D is the diffusion coefficient (m^2/s), D_0 is the preexponential factor (m^2/s), Q_d is the activation energy (J/mol), R is the gas constant (J/mol-K), and T is absolute temperature (K).

After postprocessing the aluminum composite reinforced with 6 wt.% α-Al_2O_3, the depth of diffusion should be investigated to evaluate the effect of case hardening on its bulk and surface properties. The depth of diffusion was calculated after each hour of processing by using a Gatan ion milling machine and micropolishing the sample surface for energy-dispersive spectroscopy (EDS) analysis (Renishaw). In EDS, a concentrated x-ray beam is focused onto the ion-milled surface then the backscattered electromagnetic emission spectrum is recorded using a detector to identify the elemental peaks of the case-hardened composite; similar peaks were reported by Srinivasu et al.[20]. The depth of carbon diffusion (Fig. 5) into the case-hardened AAMMC was recorded to be around 700 μm after microwave-assisted carburization at 500°C for 6 h. Extending the duration of carburization beyond 6 h had no impact on the depth of diffusion at 500°C. This phenomenon is due to the critical saturation level of the diffusion coefficient achieved, beyond which carburizing at a temperature of 500°C does not provide sufficient energy for further absorption of carbon by the composite surface. Moreover, the solubility of carbon in aluminum is less than 0.02% at temperatures near 500°C. As the processing temperature was restricted to 500°C, the diffusion did not reach a greater depth, in agreement with the formula relating the diffusion coefficient and the amount of atoms diffused, reported by Suthar et al.[22]. From Fig. 6, it is clear that the presence of carbon was observed on the surface and in the shallow subsurface of the case-hardened T6-treated AAMMC.

Figure 7(A) and (B) respectively present the x-ray photoelectron spectroscopy (XPS) results and electron diffraction pattern (EDP) of the composite surface after case hardening. The surface of the case-hardened sample was studied by XPS and the grazing-incidence diffraction method at a minimum angle of incidence of 1°. XPS analysis of the case-hardened AAMMC revealed the Al 2*p* peak at binding energies of 74.8 eV and 73.5 eV, matching with aluminum hydroxide Al $(OH)_3$. During sample preparation, the surface was ion etched for 120 s, and for the case-hardened samples, the peak for Al_4C_3 compound was seen at 284.5 eV. The electron diffraction pattern confirmed the presence of Al_4C_3,

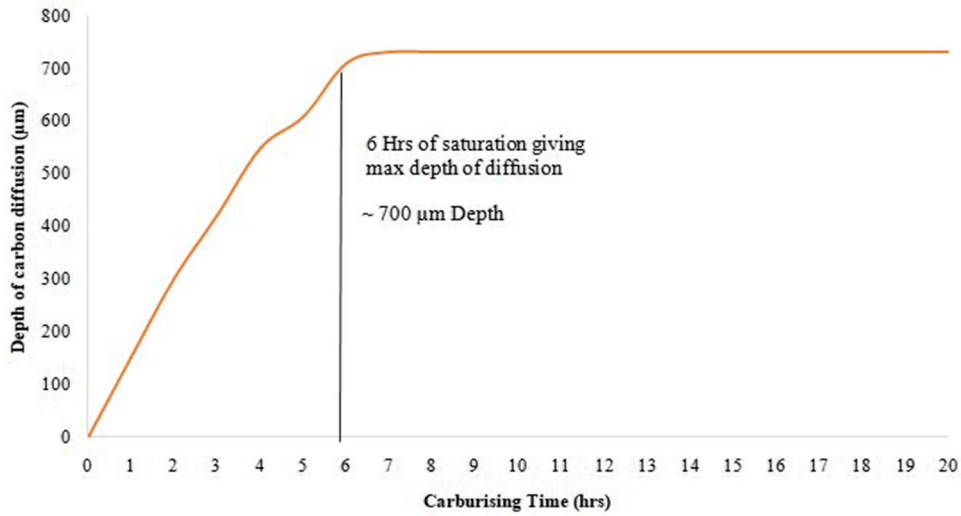

Fig. 5. Depth of diffusion recorded after case hardening.

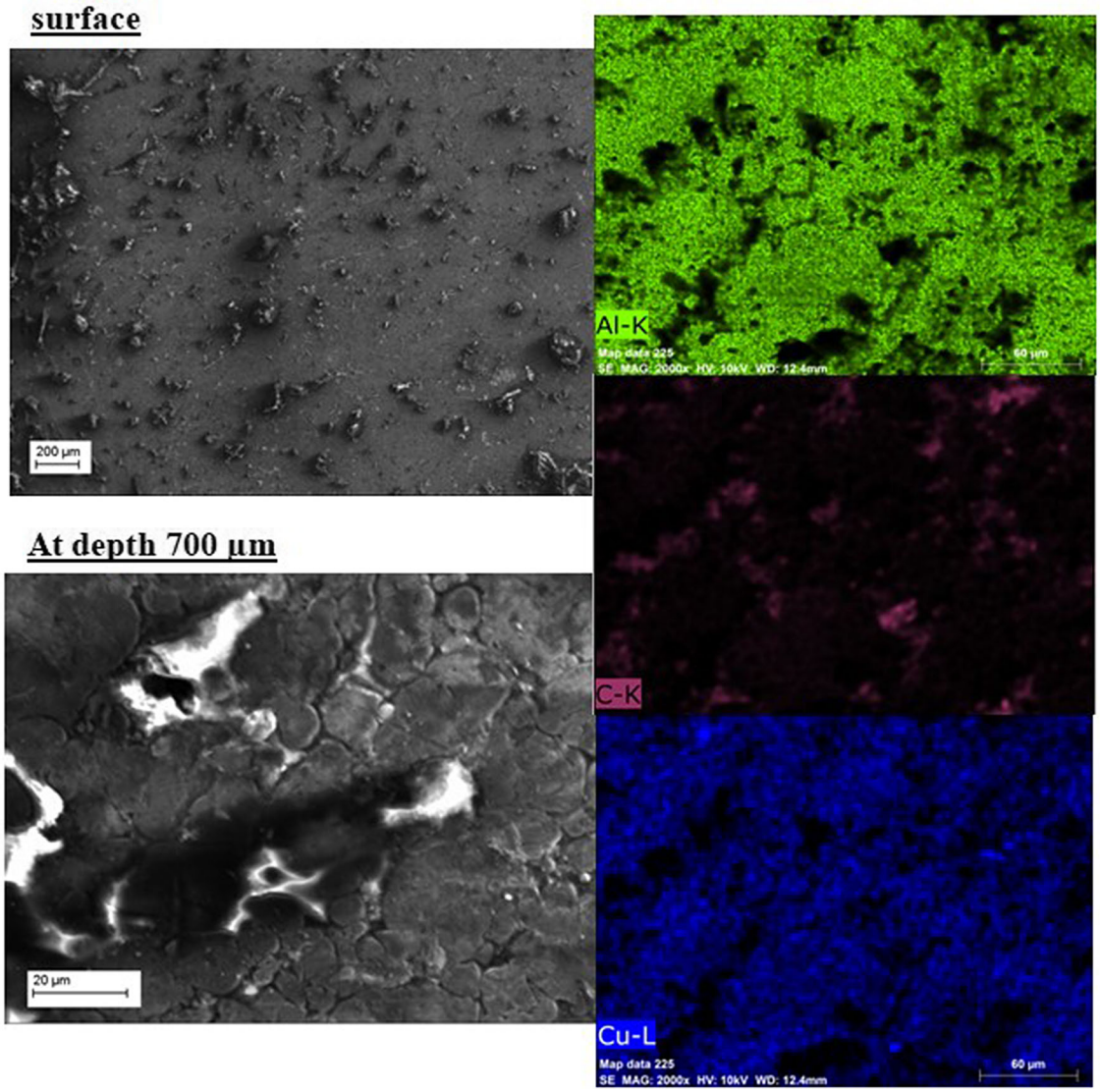

Fig. 6. EDS element mapping for case-hardened sample.

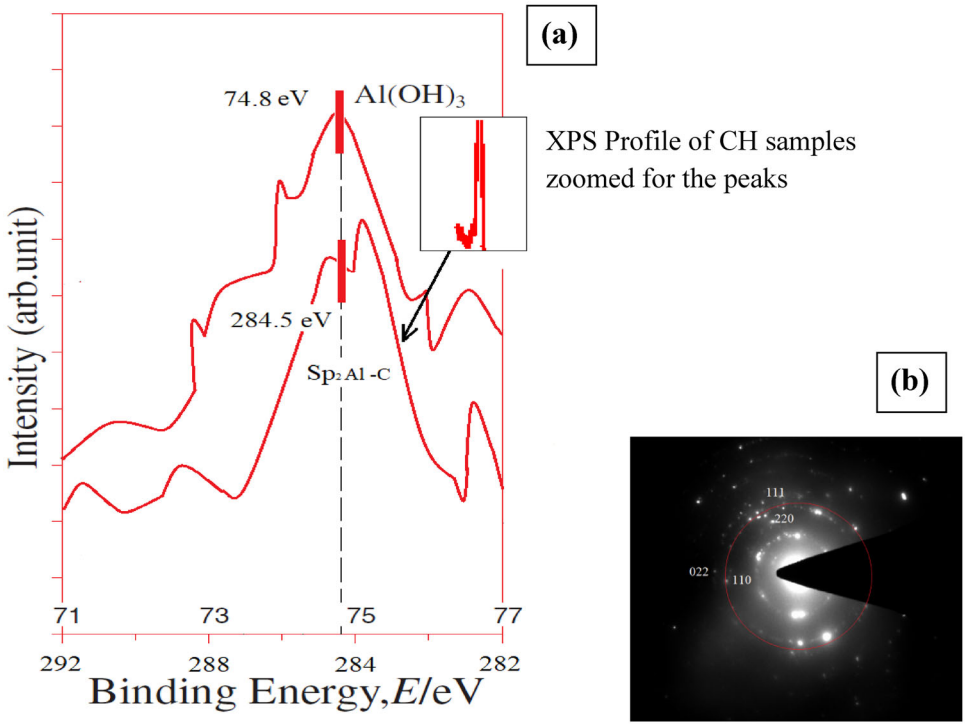

Fig. 7. (A) XPS and (B) electron diffraction pattern of case-hardened sample.

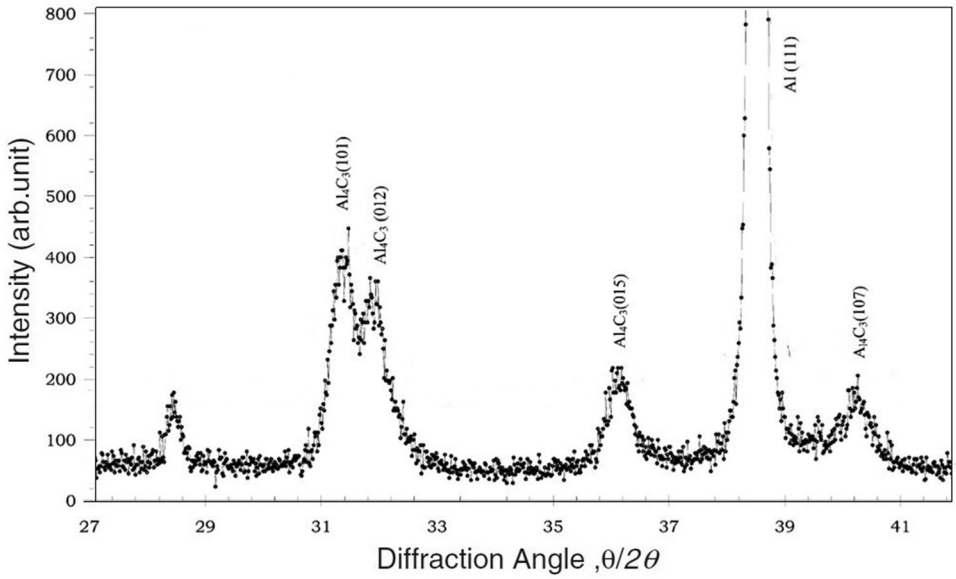

Fig. 8. XRD of case-hardened composite.

clearly possessing rhombohedral structure. In combination, the XPS, EPD, and XRD results confirm the successful formation of Al_4C_3 on the surface and in the subsurface of the composite (Fig. 8). For the case-hardened samples, the measured peaks could be indexed to the Joint Committee on Powder Diffraction Standards (JCPDS) database. The XRD patterns of the case-hardened samples exhibited peaks corresponding to aluminum, Al_4C_3 [at 2θ values of $\sim 31.14°$, $35.88°$, and $40.55°$ corresponding to (101), (012), and (107)], and trace unreacted carbon that diffused during processing. As the diffusion depth of carbon is tightly controlled by the limited temperature range used during solution treatment (i.e., 500°C), the intensity of the signal corresponding to Al_4C_3 formed after aging was found be moderate. The surface was not greatly

damaged after carburizing but was found to be rich in Al_4C_3.

Property Validation

To investigate the effect of case hardening on the surface properties of AAMMC fabricated by powder metallurgy, Vickers hardness, surface roughness, compressive strength, and shear strength evaluations were performed. Furthermore, contact characteristics of the AAMMC surface such as the thermal conductivity and wear performance were also studied to understand the effect on them. Supplementary Fig. S1(a) and (b) present the Vickers hardness data obtained to evaluate the improvement of the surface hardness, by using a Matsuzawa MMT-X Vickers hardness tester to indent the surface with a diamond tip under 500 gf with holding time of 15 s to measure the surface hardness. The average of 15 readings was recorded at a span of 100 μm and plotted in figure S1 (a) and for transverse direction the reading was recorded as shown in Supplementary Fig. S1(b). Supplementary Fig. S1(a) and (b) clearly show that the surface hardness was improved by the two different processing methods in their own ways. In the case of case-hardened (CH) samples, formation of Al_4C_3 precipitates additionally improved the surface hardness, along with the precipitates formed as an outcome of the T6 treatment and also because of the 6 wt.% α-Al_2O_3 reinforcement. This kind of surface improvement is greatly desired in AAMMC fabrication, because the requirements for brake pad applications in the aerospace field are quite demanding. Utkarshet et al.[25] reported the same type of behavior when a composite was fabricated by the powder metallurgy route, which increased its surface hardness and mechanical properties. The amount of Al_4C_3 phase formed on the surface also determines the resulting surface hardness of the AAMMC material, depending on the time and temperature. Measurements of the hardness in the transverse direction confirmed the surface diffusion of carbon atoms as discussed above, thus confirming that carbon diffusion results in good hardness values up to 700 μm for the CH samples, approaching the values for the T6-treated samples, as shown in Supplementary Fig. S1(b).

Supplementary Fig. S2 shows the stress–strain plot of the parent alloy AA 2900, T6 6 wt.% α-Al_2O_3, and T6-AAMMC CH. Supplementary Table S3 presents the ultimate compressive strength (UCS), compressive extension, and Young's modulus values of the processed AAMMC. From Supplementary Fig. S2, it is clear that the parent alloy AA 2900 without any postprocessing and addition of ceramic reinforcement exhibited a UCS value of 221 MPa and a good, ductile mode of failure, as reflected in the compressive extension value. This indicates that the pure alloy failed after bulging, a phenomenon mainly due to the higher dislocation density found in the pure alloy.

The pure alloy reinforced with 6 wt.% α-Al_2O_3 after T6 heat treatment exhibited a slightly lower compressive extension value of 2.918 mm, indicating that the dislocation density in the pure alloy was slightly reduced by such addition of α-Al_2O_3 to the ductile matrix. Moreover, the UCS of AAMMC was improved to 389 MPa (i.e., by 43.18%) when compared with the pure alloy. When α-Al_2O_3 was added to the ductile matrix, the load-bearing capacity of the AAMMC gradually increased. The homogeneous dispersion and homogenous nucleation of the added α-Al_2O_3 and nucleated Al_2Cu precipitates improved the UCS value of the AAMMC to a greater extent compared with the pure alloy (Supplementary Fig. S2) [24,26]. In the case of CH AAMMC, the depth of carbon diffusion and the quantity of Al_4C_3 formed on the surface and in the bulk determined the stress–strain behavior. In addition to the α-Al_2O_3 reinforcement and formation of Al_2Cu precipitates, the homogeneity of the Al_4C_3 on the surface after applying the CH process to AAMMC improved its UCS by 46.48% (i.e., 413 MPa) compared with pure AA 2900. This improvement in the UCS (Supplementary Table S3) of the AAMMC occurs owing to the great reduction in the dislocation density, which is further restricted by nucleation of the Al_4C_3 that occupies the boundary between the precipitate reinforcement and the matrix reinforcement. The homogeneously nucleated Al_4C_3 on the surface acts as a good toughness-bearing material that also provides additional resistant to bulging mode failure during compressive testing. This load-bearing mechanism can be achieved by surface or bulk modification of any aluminum alloy combination.

Supplementary Fig. S3 presents a SEM image of the fracture morphology of T6-AAMMC-CH after compressive testing. The depth of carbon diffusion and the quantity of Al_4C_3 formed on the surface and in the bulk determined the stress–strain behavior of the AAMMC. This improvement in the UCS of the AAMMC is due to the great reduction in the dislocation density, which is further restricted by nucleation of Al_4C_3 that occupies the boundary interface between the precipitate reinforcement and the matrix reinforcement. Thus, microwave-assisted case hardening treatment of the composites led to the formation of ultrafine grain microstructure. The resulting enormous enhancement is due to targeted nucleation of the Al_4C_3 at the grain boundary interface that forms across the surface of the composites. Thus, load transfer from the matrix to reinforcement occurs solely via interfacial bonding between them and interparticle shear stresses. Instantaneous brittle-mode fracture of the composites was observed in the near-subsurface region compared with the core bulk of the fabricated AAMMC, whereas no trace of bulging of the composites was noted during compressive loading[29]. Such ultrafine-grained microstructure plays an

important role in strengthening nanocomposites, being achieved here by employing microwave case-hardening treatment, which is considered to produce precipitation strengthening and grain-boundary strengthening according to Orowan strengthening theory. Dilipet et al. (2019) reported that homogeneously nucleated Al_4C_3 on the surface acts as a good toughness-bearing material that additionally provides resistance to bulging-mode failure, leading to the observation of rupture failure at the circumferential surface, as also seen in Supplementary Fig. S3.

Wear and Frictional Studies

The wear performance of the developed and processed AAMMC materials was validated by adopting a pin-on-disc configuration with a pin heating module. The pin-on-disc machine used to mimic the real-time braking scenario of brake pads for aerospace applications was a Ducom TR 201LE tribometer supplied by Ducom India private ltd., India. Supplementary Tables S4 and S5 present the wear performance data recorded after testing in two temperature ranges at which actual brake pads will operate (i.e., 300°C and 450°C). The input parameters were calculated from the actual braking operating conditions, viz. load of 100 N (10 kg), track diameter of 80 mm, and rotation speed of 1000 RPM. Testing was carried out in two conditions as per the standards and the braking requirements in real operating conditions. One was a continuous wear scenario while the other examined the wear performance in a given stopping distance. For the continuous wear test, the total wear distance was calculated from the runway distance required by an aircraft to land. In this context, 250 m was calculated for a single landing, with the brake pads being changed after every 120 or every 1.5 mm of total wear. To perform the validation for a given stopping distance using the processed pins, the same input conditions were selected but the power supply to the rotating disc was stopped so that the pin in contact applied a load of 100 N and tried to stop the disc, with the stopping time and distance being recorded using a stopwatch and tachometer. The stopping distance of the aircraft was then calculated by considering the required landing distance (Supplementary Fig. S4). In the current research, the requested stopping distance was set at approximately 250 m. The stopping distance was calculated using Eq. (3) after the test [26].

$$\text{Stopping distance} = \frac{\text{Velocity}^2}{2\,(\text{Coefficient of friction})\,(\text{Gravitaional acceleration})} \quad (3)$$

where d is the stopping distance (m), v is the velocity (m/s), μ is the coefficient of friction (CoF), and g is the acceleration due to gravity (9.8 m/s^2).

The results presented in Supplementary Tables S4 and S5 indicate that the lower CoF was recorded for the T6-AAMMC CH samples, which exhibited lower frictional force at the contact interface, leading to the higher CoF. After prolonged exposure to 450°C, the Sn content in the matrix alloy acted as a solid lubricant at the interface, reducing the CoF and eventually the frictional force at the interface, as also reported by Suthar et al.[22]. T6-AAMMC also exhibited clean and steady CoF without any fluctuation throughout the test duration. This phenomenon is in good agreement with the earlier discussion regarding the density and hardness, because microwave-assisted heat treatment of AAMMC provided good interparticle bonding, which made the composite surface firm with uniformly nucleated Al_2Cu. Homogeneously dispersed α-Al_2O_3 and uniformly nucleated Al_2Cu exhibited consistent CoF. It is very clear that the highest wear in microns was recorded for the samples that were T6 processed. The lowest wear was recorded for T6-CH samples. All the wear and CoF results are in good agreement with earlier findings. Note that case hardening of AAMMC significantly improved the properties of the resulting material, which performed the same as expected based on the benchmark material.

Supplementary Fig. S5 presents SEM micrographs of samples that were tested for continuous wear and stopping distance. After testing in both modes, the surface exhibited severe seizure damage because of the high average surface roughness after the processing. Higher surface roughness of the samples leads to high frictional force, which causes a higher CoF and poor wear performance. This phenomenon is not seen in the wear data presented in Supplementary Tables S4 and S5, where the lowest wear was recorded for the T6-CH samples in comparison with other processing conditions. This is supported by the surface seizure and particle abrasive wear that was observed initially at the start of the wear process, and later because the presence of Al_2Cu and added α-Al_2O_3 dispersed on the subsurface stabilizes the total induced wear. The Al_4C_3–Al_2Cu–α-Al_2O_3 combination is observed to be quite dominant in improving the wear resistant of the material. Sn alloyed in the matrix metal also facilitated a reduction in the wear to some extent by creating a protective layer at the interface, thus reducing the frictional force generated and eventually reducing the total wear. On the case-hardened wear surface, the self-adhesive wear mechanism was observed, as a result of which the composite surface was spotted with plastic deformations containing Al_4C_3–α-Al_2O_3 clusters. The formation of the cluster was observed in the direction opposite to the sliding direction. No evidence of abrasive wear was observed on the composite surface. Very little fragmentation of debris particles was observed on the surface after continuous wear testing. As the entire process was carried out at 300°C or 450°C,

self-adhesion was observed on the surface where the material flows.

Supplementary Fig. S6(a) presents the surface roughness topography as observed by atomic force microscopy (AFM) on pure AA 2900 alloy tested using the stopping distance criterion. The topography clearly shows that the observed mode of surface wear is mostly adhesive wear. The AFM topography clearly displays a pile of material in the opposite direction to the sliding direction, leading to adhesive wear.

From Supplementary Fig. S6(b), it is clear that T6-AAMMC after microwave-assisted heat treatment exhibited grain-boundary precipitation and encapsulation of α-Al_2O_3 particles, which leads to the least particle pull-out from the surface even after testing in extreme conditions (i.e., 100 N). No severe surface seizure and deep grooves or plowing mechanism of the added α-Al_2O_3 particles were noted after testing in the stopping distance mode. According to Supplementary Fig. S6(c), the surface after stopping distance testing exhibited severe seizure damage because of the high average surface roughness recorded after the processing. The higher surface roughness of the samples led to a high frictional force, which leads to higher CoF and poor wear performance. This phenomenon is not seen in the wear graph presented in Supplementary Fig. S6(a), where the lowest wear was recorded for the T6-CH samples compared with other processing conditions. This is supported by the surface seizure and particle abrasive wear that was observed initially at the start of the wear process, and later because of the presence of Al_2Cu and added α-Al_2O_3 dispersed on the subsurface, stabilizing the total induced wear. The Al_4C_3–Al_2Cu– α-Al_2O_3 combination is observed to be quite dominant in improving the wear resistant of the material, as seen from Supplementary Fig. S6(a). Sn alloyed in the matrix metal also facilitated the wear reduction to some extent by creating a protective layer in the interface and thus reducing the frictional force generated, eventually reducing the total wear. An overall summary of these findings is presented in Supplementary Fig. S6.

CONCLUSION

Homogeneous dispersion of α-Al_2O_3 plus microwave-assisted T6 heat treatment resulted in good reinforcement–precipitate–matrix interfaces. Case hardening of the composite resulted in good structural integrity with α-Al_2O_3 retained, thereby improving the mechanical properties. Substantial improvements in surface properties such as the microhardness and wear performance (up to 500 μm depth) were achieved for the prepared composites with the surface modified by case hardening. The case-hardening process formed Al_4C_3 on the surface, which was found to be present in significant amounts, thus improving the surface properties. Significant improvements in the hardness (i.e., 17.5% for CH samples) and compressive strength (i.e., 5.8% for CH samples) due to Al_2O_3 addition and the surface modification process were observed. Case hardening of the Al_2O_3 composite offers the advantages of reducing both the wear loss (i.e., 0.55 mm for CH) as the well friction coefficient (i.e., 0.326 for CH samples). The evaluation of the processed composites versus the properties of existing brake pad materials revealed similar performance. In comparison with the properties of actual brake pad materials, the developed composite material exhibited improvements in the compressive strength (i.e., 27% for CH samples), surface hardness (i.e., 13% for CH samples), and shear strength (i.e., 12% for CH samples). The wear loss and CoF of the developed composites lay in regimes close to the benchmark material used in aerospace brake pads. The case-hardened samples endured for 92 landings, representing almost 76.6% of the required performance.

CONFLICT OF INTEREST

The authors declare that they have no known competing financial interests or personal relationships that could have appeared to influence the work reported in this paper.

SUPPLEMENTARY INFORMATION

The online version contains supplementary material available at https://doi.org/10.1007/s11837-021-04925-2.

REFERENCES

1. M.K. Abbass, *Lasers Manuf. Mater. Process.* 5, 81. (2018).
2. Alexander Katz-Demyanetz, Vladimir V. Popov Jr, Aleksey Kovalevsky, Daniel Safranchik, Andrey Koptyug, Manuf. Rev., 6 (2019).
3. B. Bobić, S. Mitrovic, M. Babic, and I. Bobic, *Tribol. Ind.* 32, 3. (2010).
4. DilipRaja, Selvamani S T., Vigneshwar M., Palanikumar K., Velu R., Mater. Today Proc., 16, 1279 (2019).
5. C. Elanchezhian, R.B. Vijaya, G. Ramakrishnan, R.K.N. Sripada, M. Mithun, and V. Kishore, *Mater. Today Proc.* 5, 1211. (2018).
6. F. Kiyoshi, *Surf. Coat. Technol.* 133, 264. (2000).
7. Y.-Y. Gao, *Mater. Charact.* 141, 156. (2018).
8. Ikumapayi, Omolayo M., Esther T. Akinlabi, Mater. Res. Exp, 6, 076546 (2019).
9. Kavi K V., Swathi V., Thayalan K., Sabbir Ahmed, Mohan K P., Mater. Res. Exp, 6 (2019).
10. A. Kurt, I. Uygur, and E. Cete, *J. Mater. Process. Technol.* 211, 313. (2011).
11. MadevaNagaral, Shivananda B K., Virupaxi A., Kori S A., Stren. Frac. Comp, 13, 1 (2019).
12. ManishShukla, Dhakad S K., Pankaj Agarwal., Mohan Kumar P., Mater. Today Proc., 5, 5830-5836 (2018).
13. MiranMozetič, Materials, 12, 441 (2019).
14. G. Murtaza, S.S. Hussain, M. Sadiq, and M. Zakaullah, *Thin Solid Films* 517, 6777. (2009).
15. S.V. Prasad, and R. Asthana, *Tribol. Lett* 17, 445. (2004).

16. Prem ShankarShau, Banchhor R., Int. Res. J. Eng. Technol., 3, 123 (2016).
17. S.J. Huang, A. Muneeb, A. Abbas, and R. Sankar, *J. Mater. Res. Technol.* 11, 1424. (2021).
18. V.K. Sharma, Vinod Kumar, Ravinder Singh Joshi. *J. Mater. Res. Technol.* 8, 3504. (2019).
19. Snihirova D, SV. Lamaka, F Montemor, Smart Comp. Coatings Mem., 85 (2016).
20. Srinivasu, R., Sambasiva Rao A., Madhusudhan Reddy G., Srinivasa RaoK., Def. Technol., 11, 140 (2015).
21. S. Singh, and K. Pal, *Mater. Sci. Eng. A* 644, 325. (2015).
22. Suthar Jigar, Patel K M., Mater. Manuf. Process., 33, 499 (2018).
23. Toozandehjani Meysam, Kamarudin N B., Zahra D., Yee E L., Ashen G., Chandima G., Am. J. Aero. Eng., 5, 9 (2018).
24. P. Ashwath, and M. *Anthony Xavior. Proc. Eng.* 97, 1027. (2014).
25. Utkarsh Pandey, Rajesh Purohit, Pankaj Agarwal, Dhakad S K., Rana R S., Mater. Today Proc., 4, 5452 (2017).
26. Ashwath, P., Joel, J., Jeyapandiarajan, P., Xavior, A., and Rajendran, R., Mater. Res. Exp., 7 (1), 016509 (2019).
27. Logesh, K., Hariharasakthisudhan, P., Moshi, A. A. M., Rajan, B. S., and Sathick basha, K. Mater. Res. Exp., 7 (1), 015004 (2019).
28. Granesan, S., Ganesh, S. D., & Moshi, A. A. M. IOP Conf. Ser. Mater. Sci. Eng, 988, 1, 012029 (2020).
29. A. Abbas, and S.J. Huang, *JOM* 72(6), 2272. (2020).